Journal of
Water & Climate Change

IWA PUBLISHING

Journal of Water and Climate Change Vol 14 No 4, 1339 doi: 10.2166/wcc.2023.507

Assessing the performance of daily to subdaily temporal disaggregation methods for the IDF curve generation under climate change

Fahad Alzahrani [a,b], Ousmane Seidou [a] and Abdullah Alodah [c,*]

[a] Department of Civil Engineering, College of Engineering, University of Ottawa, 75 Laurier Ave. E, Ottawa, ON K1N 6N5, Canada
[b] Department of Hydrology and Water Resources Management, Faculty of Meteorology, Environment and Arid Land Agriculture, King Abdulaziz University, Jeddah 80208, Saudi Arabia
[c] Department of Civil Engineering, College of Engineering, Qassim University, Buraydah, Al Qassim 51431, Saudi Arabia
*Corresponding author. E-mail: aalodah@qu.edu.sa

FA, 0000-0003-2593-6190; OS, 0000-0003-1706-0176; AA, 0000-0002-0815-4579

ABSTRACT

Given the short concentration time in urban watersheds, the design of municipal water infrastructures often requires knowledge of sub-daily precipitation intensity. Sub-daily time series can be directly used in a rainfall–runoff model or to derive intensity–duration–frequency (IDF) curves and calculate the design precipitation. Given that precipitation projections are typically at a daily time scale, temporal disaggregation using techniques of variable complexity is often needed to evaluate the risk/performance of urban infrastructure in the future. This paper proposes a simple steady-state stochastic disaggregation model that generates wet/dry day occurrence using a binomial distribution and precipitation intensity using an exponential distribution. Daily precipitation data from four regional climate models (RCMs) forced with the high-emission scenario representative concentration pathway (RCP 8.5) were downscaled using the quantile mapping (QM) method. The performance of the developed method is compared to widely used temporal disaggregation methods, namely, the multiplicative random cascade model (MRC), the Hurst–Kolmogorov process (HKP), and three versions of the K-nearest neighbour (KNN) model, using the Kolmogorov–Smirnov (KS) test. The six disaggregation techniques were assessed at four stations in the South Nation River Watershed in Eastern Ontario, Canada. Results indicate that, despite its simplicity, the proposed method performed well compared to other temporal disaggregation methods when resampling the observed extreme precipitation.

Key words: climate change, FO method, IDF curves RCM, temporal disaggregation

HIGHLIGHTS

- Climate change impacts on short-duration precipitation extreme events are investigated using different temporal disaggregation methods.
- A simple steady-state stochastic disaggregation model is introduced to generate future sub-daily precipitation intensities.
- The developed disaggregation method adequately resamples the observed short-duration extreme precipitation for application in municipal water infrastructures.

GRAPHICAL ABSTRACT

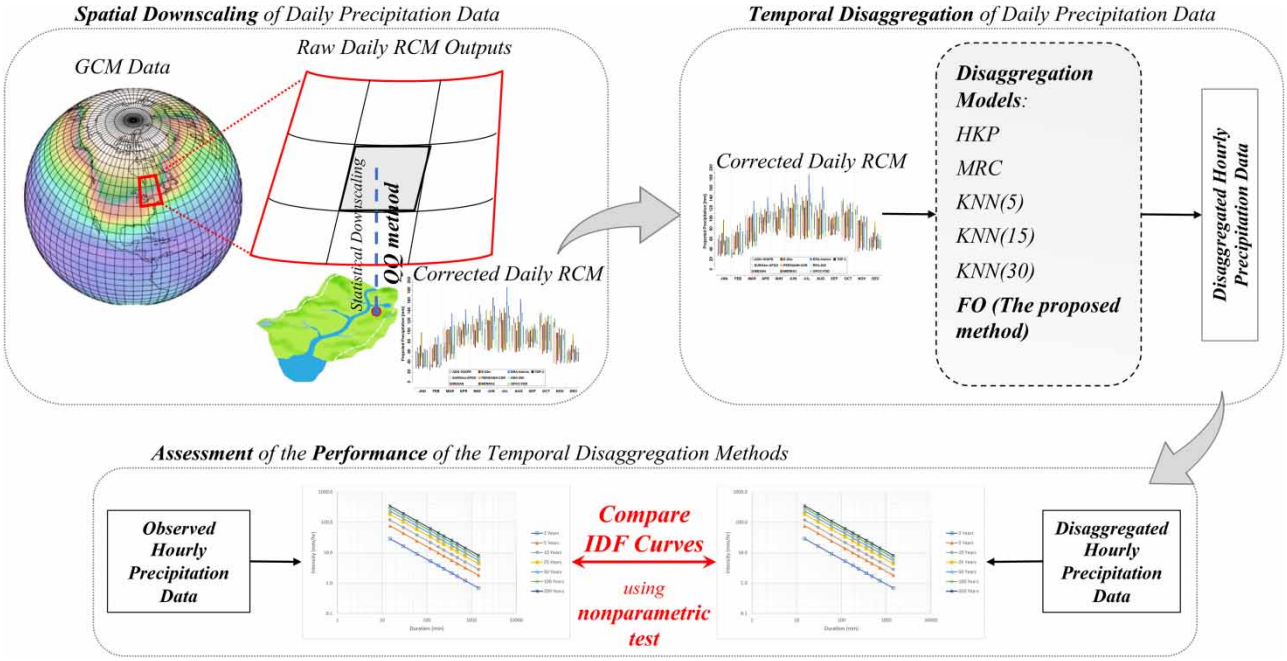

1. INTRODUCTION

Changes in the temporal variability of precipitation at all timescales are expected due to global warming. Such changes affect urban water infrastructure by potentially influencing its performance and risk of failure. Unfortunately, there is considerable uncertainty about how hydrological variables will change in the future. While uncertainty is present at all timescales, the climate signal in the daily time series simulated by climate models, for instance, can be estimated with much greater certainty than in the simulated hourly time series (Jakob *et al.* 2011). Sub-daily (fine-scale) time series are critical in some water resource engineering problems, especially for local hydrological evaluations in a changing climate (Zhu *et al.* 2012). One way of obtaining hourly or sub-hourly precipitation times in the future is to temporally disaggregate daily time series generated using either weather generators or downscaling climate model outputs. Daily time series can be disaggregated into hourly time steps and converted to intensity–duration–frequency (IDF) curves or be directly fed to a rainfall–runoff model (Alzahrani *et al.* 2022). For instance, Zhao *et al.* (2021) proposed a framework for constructing future IDF curves for tropical cities in Southeast Asia. It consists of bias-correcting daily regional climate model (RCM) outputs using a version of the quantile mapping (QM) method, temporally downscaling it, and generating IDF curves. Temporal disaggregation is the conversion of annual, monthly, or daily scale observations into sub-daily scales, such as hourly or minute scales, using a stochastic or machine learning approach. Examples of temporal disaggregation techniques include (i) the K-nearest neighbour disaggregation model (KNN); (ii) the multiplicative random cascade model (MRC); (iii) the microcanonical random cascade model (MRCM) (Olsson 1998; Olsson & Berndtsson 1998; Molnar & Burlando 2005; Licznar *et al.* 2011; Jebari *et al.* 2012; Müller & Haberlandt 2015; Garbrecht *et al.* 2017; Gaur & Lacasse 2018); and (iv) the Hurst–Kolmogorov process (HKP) downscaling model (Hurst 1951; Koutsoyiannis & Cohn 2008; Müller & Haberlandt 2015; Lombardo *et al.* 2017).

The KNN disaggregation technique is a version of the method of fragments (MF). The MF is a popular nonparametric temporal disaggregation approach in which sub-daily precipitation values are estimated as fractions (fragments) of the daily precipitation amount. In the KNN approach, the fragments are calculated using available daily and hourly precipitation time series that are close (neighbour) to the period of interest based on a distance measure (e.g., distance in time, magnitude, etc.). Park & Chung (2020) applied the KNN model using 3-day patterns and found that the disaggregated hourly rainfall data had similar statistical properties to the observed series. Sharif *et al.* (2013) applied the KNN model to synthesize and temporally disaggregate daily precipitation under climate change scenarios in the Upper Thames River Basin (UTRB). They found that the model effectively reproduces simulated sequences of future climate scenarios represented and predicted by

Global Climate Models (GCMs). Lu *et al.* (2015) investigated the effects of climate change on heavy regional rainfall by producing a spatially and temporally varying rainfall time series using a hybrid stochastic weather generator (LARS-WG) and a KNN model. Uraba *et al.* (2019) used a stochastic KNN disaggregation model to convert downscaled GCM scale rainfall production; they found that climate change's impact on rainfall intensity would be noticeable in storms with shorter durations and longer return times. Sharma & Srikanthan (2006) applied KNN combined with the fragment (KNN–MOF) method. Their results showed that the KNN–MOF performed better in producing the descriptive statistics of wet and dry spell distributions than the other models. The main challenge in the KNN model is choosing the optimum value of neighbours for the temporal downscaling process. The number of neighbours should be estimated to synthesize daily time series using the KNN model (Sharif & Burn 2007).

HKP is a stochastic process disaggregation model that uses Gaussian white noise to convert precipitation from coarser to finer scales. This model uses the Hurst exponent (H) to qualify the data behaviour. Hurst (1951) observed randomness in numerous physical time series, and the tendency of natural events was the most significant even though these events were in higher and lower values. The HKP method was intensely used in hydrology and water resource management to generate sub-hourly or sub-daily scales for different purposes in the urban water system. A challenge in the HKP model is determining the H value, which is expensive to estimate. Lombardo *et al.* (2012) used HKP to convert the daily precipitation into a 5-min time step. However, the model is in the log domain and not all daily time series are appropriate for a lognormal distribution.

The MRC model, first introduced by Olsson (1998), is an invariance scaling method used for temporal downscaling. Gaur & Lacasse (2018) applied the MRC model to multivariate climate variables at several sites within the same region to assess the model's accuracy in performance. Licznar *et al.* (2011) generated a fine-scale using the multiplicative cascade model and a microcanonical cascade, yielding intermittency on a 5-min scale. Molnar & Burlando (2005) found that the cascade model performed well in terms of rainfall distribution preservation at a 10-min scale; the model could reproduce the growth of the intermittency period. Koutsoyiannis & Onof (2001) developed a stochastic disaggregation model that combines a precipitation simulation with an adjustment process to convert the coarse-scale to a finer-scale. This model's main advantage is preserving descriptive precipitation statistics; however, its main limitation is that the model does not reproduce instantaneous hourly series because of the variance in the generated weights in each cascade level. Müller & Haberlandt (2015) found that a 5-min resolution will lead to missing time steps with dry intervals if the branching of the cascade is constant and this is generally considered a limitation for the cascade model.

Temporal disaggregation techniques have different levels of complexity and unequal performances and the generated time series may not have the same statistical characteristics (Tayşi & Özger 2022). HKP and MRC are mathematically challenging to calibrate, while the KNN methods are straightforward. A natural question is whether more complex temporal disaggregation techniques lead to better results regarding IDF curves and descriptive statistics of the disaggregated time series. In this paper, a simple temporal disaggregation technique called the Fahad–Ousmane (FO) method is introduced. Daily time series of future precipitation are generated by spatially downscaling the outputs of four RCMs using the QM method. It has only two parameters and its calibration is straightforward compared to HKP and MRC. The FO model and five alternative temporally downscaling methods (the MRC, the HKP, and three versions of the KNN) are used to generate hourly precipitation time series in both the historical (1976–2005) and future periods (short-term 2010–2040, medium-term 2041–2070, and long-term 2071–2100). Besides the visual comparison of generated IDF curves, the two-sample Kolmogorov–Smirnov (KS) test is used to compare the distribution of the time series of annual precipitation of durations 1 and 24 h.

2. MATERIALS AND METHODOLOGIES

2.1. General methodology

The general methodology of the work, as illustrated in Figure 1, is described as follows:

- Developing a simple temporal disaggregation technique called the FO method
- Generating daily precipitation time series by downscaling the nearest grid data of a climate model's precipitation output using the QM method
- Disaggregating these time series from daily to sub-daily (hourly) timescales by the MRC, the HKP, three versions of the KNN (5, 15, and 30), and the FO model

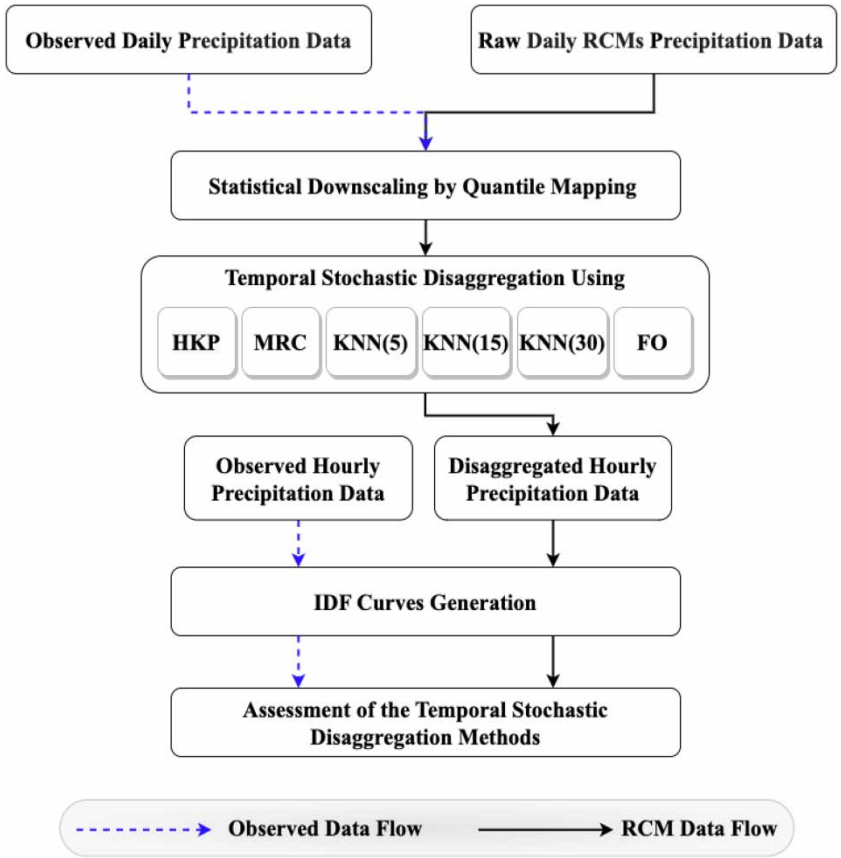

Figure 1 | Flowchart of the adopted methodology of this work.

- Extracting the maximum annual precipitation intensity for durations of 1–24 h from the disaggregated and observed time series
- Generating IDF curves from the maximum annual precipitation of the disaggregated and observed time series
- The disaggregation performance was tested using visual comparisons, main statistics, and the two-sample KS test

2.2. Study area and available data

The study area is the South Nation watershed (approximately 4,000 km^2), located southeast of Ottawa in Eastern Ontario, Canada (Figure 2). The South Nation River drains the watershed for 175 km with relatively flat topography (approximately 80 m between its headwaters and output at the Ottawa River), making the area prone to significant flooding risk. The observed daily precipitation (PCP) and hourly precipitation acquired from Environment Canada cover the 1976–2005 period at four stations, as presented in Table 1. Table S1 (Supplementary Materials) presents the available daily outputs of several RCMs from the NA-CORDEX experiment forced with a high Representative Concentration Pathway (RCP 8.5) greenhouse gas emission scenario. The available horizontal spatial resolution, namely the North America Domain (NAM-44) (0.44°) with an approximately horizontal projected grid resolution of 50 km, was used.

2.3. Downscaling RCM outputs at the daily timescale

The outputs of the RCMs are downscaled using the QM technique. The QM method consists of remapping the probability density function (PDF) of the uncorrected RCM series in combination with the probability of the observed data series. The following formula transforms the corrected RCM to cumulative distribution functions:

$$X_{\text{Corrected}} = F^{-1}_{\text{Observed}}(F_{\text{RCM}}(X_{\text{RCM}})) \quad (1)$$

where $X_{\text{Corrected}}$ is the projected time series, F^{-1}_{Observed} is the inversed cumulative density probability, F_{RCM} is the cumulative density probability, and X_{RCM} is the RCM data before projection. In practice, Equation (1) is replaced by the following

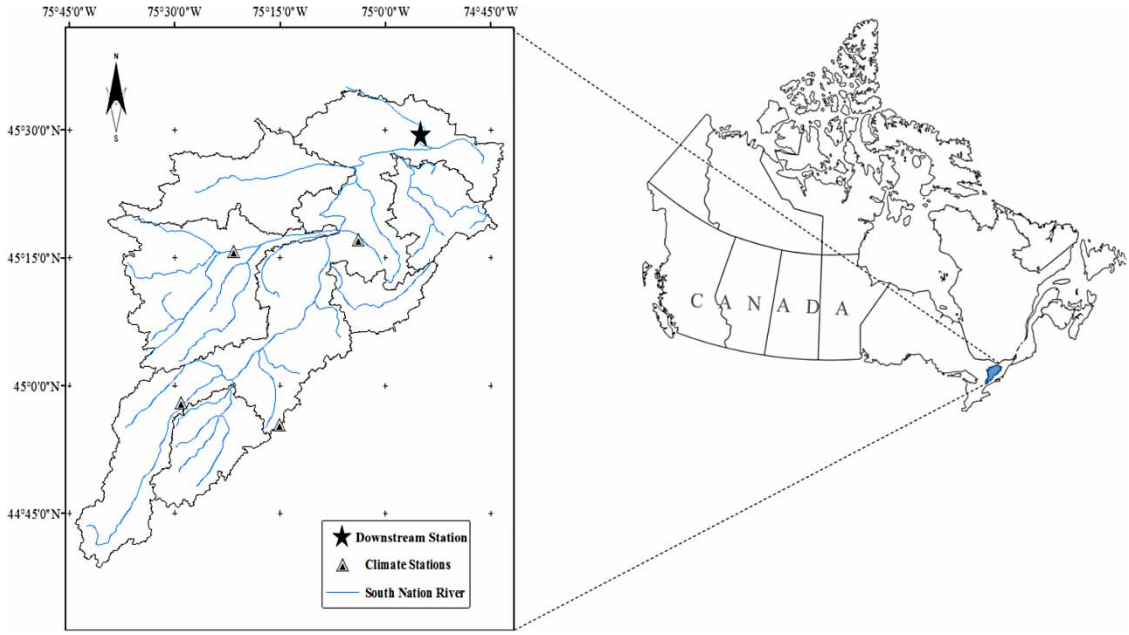

Figure 2 | The meteorological gauges in the South Nation watershed (Alodah & Seidou 2019).

Table 1 | Weather station information

Station	Latitude (N)	Longitude (W)	Elevation (m)	Mean daily PCP (mm)	Standard Deviation of daily PCP (mm)
St. Albert	45° 17′ 14″	75° 03′ 49″	80	2.77	6.06
South Mountain	44° 58′ 00″	75° 29′ 00″	84.7	2.64	6.07
Morrisburg	44° 55′ 25″	75° 11′ 18″	81.7	2.77	6.17
Russell	45° 15′ 46″	75° 21′ 34″	76.2	2.63	5.97

mapping function between GCM outputs and observations:

$$\begin{bmatrix} (X_{\text{observation}})_{\text{sorted},1} & (X_{\text{RCM}})_{\text{sorted},1} \\ (X_{\text{observation}})_{\text{sorted},2} & (X_{\text{RCM}})_{\text{sorted},2} \\ \vdots & \\ (X_{\text{observation}})_{\text{sorted},N} & (X_{\text{RCM}})_{\text{sorted},N} \end{bmatrix} \tag{2}$$

where $X_{\text{observation}}$ is the observed time series and X_{RCM} is the raw time series obtained from the climate model.

The limitation of this approach is that it cannot predict values beyond the range of historical data. The reference period is split between validation and calibration. Equation (2) is fitted to the calibration period and applied to the validation and future periods. To avoid any bias resulting from oscillations in the observed precipitation time series, the calibration data set contains all data series from 1976 to 1991, and the validation period covers the data series for the time range of 1992–2005.

2.4. Temporal disaggregation techniques

The following subsections describe the models and theories of each temporal stochastic disaggregation method. Four temporal downscaling techniques are considered: the KNN disaggregation technique, the MRC model, the HKP downscaling model, and a novel disaggregation technique called the FO model.

2.4.1. KNN disaggregation technique

KNN is a particular case of the fragment (MF) method, a nonparametric approach commonly used by researchers because of its simplicity. The principle of the method is to generate fragments that are fractions of daily precipitation that occur in each hour of the day and then, the fragments are summed to 1. The general formulation of the MF is given in Equations (3) and (4). Equation (3) contains w_i, the weight that will be computed, h_i is the data selected to produce fragments from the series, and n is the number of data in the series (24 h).

$$w_i = \frac{h_i}{\sum_{i=1}^{n} h_i} \tag{3}$$

Then, each fragment is multiplied by the daily data d in Equation (3) to obtain the new hourly data or disaggregated values.

$$h_i' = w_i \times d \tag{4}$$

The hourly series of data used to estimate fragments could be chosen randomly; however, this would lead to inadequate statistical properties (Srikanthan *et al*. 2006). Therefore, the best choice is to compare the total disaggregated daily precipitation with the close total daily precipitation before the disaggregation process (Wey 2006). The KNN is a particular case of the fragment method, where the fragment is selected from historical hourly precipitation in a sample of neighbours with similar precipitation amounts. The neighbours are selected in a temporal window to preserve the seasonal characteristics of precipitation. Note that the sliding window is based on the Julian calendar and spans all years in the data. The K neighbours with the most negligible difference in precipitation amount are selected. Then, one neighbour is sampled from the set and used to calculate the fragment. The probability of sampling neighbour $\boldsymbol{j}$ is

$$p(j) = \frac{\frac{1}{|P(j)-P(t)|}}{\sum_{i=1}^{k} (|P(i) - P(t)|)} \tag{5}$$

where $p(j)$ is the precipitation amount of neighbour j and $P(s)$ is the precipitation amount on the simulation day.

2.4.2. FO disaggregation model

FO is a steady-state stochastic disaggregation model that generates wet hours (hours with precipitation above 1 mm) using a binomial distribution with parameter p, and for each wet hour, precipitation intensity is generated using an exponential distribution with parameter α. The parameters are fitted month by month using observed data in the calibration period as follows:

(a) Estimate all hourly precipitation for month M.
(b) Estimate p as the ratio of hours with precipitation higher than 1 mm to the total number of hours.
(c) Create a time series of hours with precipitation above 1 mm.
(d) Fit the exponential distribution to the above time series to obtain α.

The generation of hourly precipitation for a day with precipitation amount p_{day} is calculated as follows:

(a) If $p = 0$, set all hourly values to 0.
(b) If $p > 0$,
    a. Generate a series of 0 (dry hours) and 1 (wet hours); repeat until you obtain at least one nonzero value.
    b. For each wet hour h, take a sample from the exponential distribution with the parameter α to obtain $p_{\text{h}}(\text{h})$; otherwise, set $p_{\text{h}}(\text{h})$ to 0 for dry hours.

The final precipitation for each hour of the day is set to

$$p_{\text{day}} = \frac{P_{\text{h}}(\text{h})}{\sum_{i=0}^{24} P_{\text{h}}(i)} \tag{6}$$

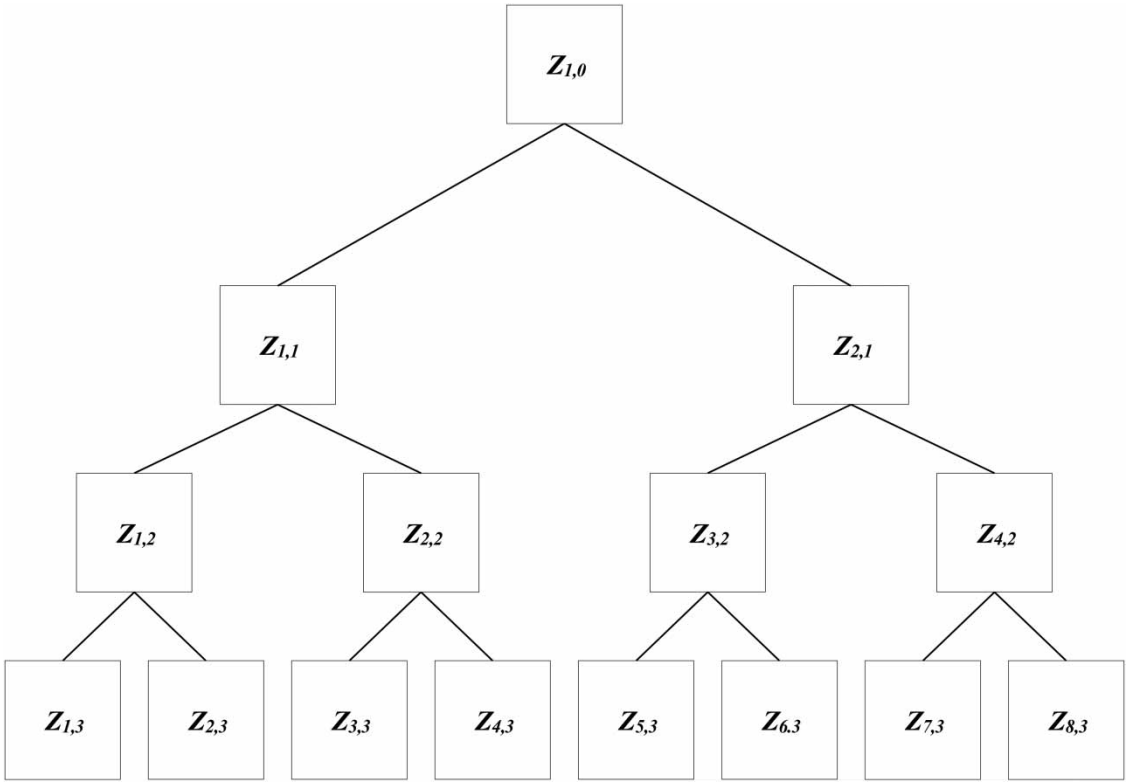

Figure 3 | A sketch of the disaggregation model steps at the level of k (Lombardo *et al.* 2012).

2.4.3. Hurst–Kolmogorov downscaling model

HKP is a technique that converts coarse-scale data into fine-scale data. This model uses pure downscaling to generate precipitation based on fractional Gaussian noise, called the HKP (Koutsoyiannis 2002). As shown in Figure 3, a dyadic additive cascade is used to disaggregate fractional Gaussian noise; each higher amount of precipitation is disaggregated into a lower-scale level. Then, the disaggregated fractional Gaussian noise is exponentially transformed to derive the actual precipitation. The HKP represents the long-term persistence of the observed time series with a simple and efficient stochastic process. Additionally, it has been demonstrated that this random representation is not solely based on data, as the behaviour of Hurst–Kolmogorov develops from entropy production (Koutsoyiannis *et al.* 2011). For any integers i and j and any timescale $\boldsymbol{f}$ and $\boldsymbol{i}$, the HKP could be defined as a stochastic stationary process, as in the following equation:

$$(\tilde{R}_j^{(f)} - \tilde{\mu}) \overset{\text{def}}{=} \left(\frac{f}{l}\right)^{H-1} (\tilde{R}_j^{(l)} - \tilde{\mu}) \tag{7}$$

where $\overset{\text{def}}{=}$ indicates the equality in probability distributions, H is the Hurst coefficient in the range between 0 and 1, $\tilde{R}_j$ is the Gaussian noise, and $\tilde{\mu} = \langle \tilde{R} \rangle$ is the mean value. For the related process, $\tilde{R}_j^{(f)}$ in the following equation is used:

$$var[\tilde{Z}_j^{(f)}] = f^2 var[\tilde{R}_j^{(f)}] = f^{2H}\tilde{\sigma}^2 \tag{8}$$

where $var[\tilde{R}] = \tilde{\sigma}^2$.

The HKP is implemented as follows: consider the Z_1^f to be the depth of daily precipitation aggregated in an enormous timescale ($j = 1$). Z_1^f is assumed to be a random variable with a mean and standard deviation of the stochastic process. The observed daily precipitation is assumed to be a lognormal distribution. An auxiliary Gaussian random variable

$Z_1^f := ln(Z_1^f)$ of the aggregated HKP on a timescale f with mean $\tilde{\mu}_0$ and variance $\tilde{\sigma}_0^2$ is expressed as in the following equations:

$$\tilde{\mu}_0 = \ln \mu_0 \ - \frac{1}{2}\left(\frac{\sigma_0^2}{\mu_0^2} + 1\right) \tag{9}$$

$$\tilde{\sigma}_0^2 = \ln\left(\frac{\sigma_0^2}{\mu_0^2} + 1\right) \tag{10}$$

$\tilde{Z}_{1,0}$ is disaggregated as a dyadic ($b = 2$) additive cascade. Then, $\tilde{Z}_{1,0}$ is split into two ($b = 2$) Gaussian random variables based on the timescale $\Delta s = f/2$. For example, at the first cascade level $k = 1$, we have $\tilde{Z}_{1,1} + \tilde{Z}_{2,1} = \tilde{Z}_{1,0}$. Similarly, the k cascade level corresponds to $\Delta s_k = 2^{-k} f$

$$\tilde{Z}_{1,0} + \tilde{Z}_{2j,k} = \tilde{Z}_{j,k-1} \tag{11}$$

Consequently, the equation is adequate to generate $\tilde{Z}_{j,k-1}$ and then obtain $\tilde{Z}_{2j,k}$.

This is a generic procedure that resembles the well-known interpolation procedure. Therefore, the following linear generation scheme is considered, as shown in Figure 3:

$$\tilde{Z}_{2j-1,k} = \ \theta^T Y + V \tag{12}$$

where $V = [\tilde{Z}_{2j-3,k}, \tilde{Z}_{2j-2,k}, \tilde{Z}_{j,k-1}, \tilde{Z}_{j+1,k-1}]^T$, Θ is a vector of parameters, and V is Gaussian white noise. This equation allows the interpolated value to preserve the total depth of two earlier lower-level variables (level k) and one later higher-level variable (level $k-1$) (Koutsoyiannis 2002).

Therefore, in each disaggregation step, two lower-level variables are estimated by

$$\tilde{Z}_{2j-1,k} = a_2\tilde{Z}_{2j-3,k} + a_1\tilde{Z}_{2j-2,k} + b_0\tilde{Z}_{j,k-1} + b_1\tilde{Z}_{j+1,k-1} + V \tag{13}$$

$$\tilde{Z}_{j,k-1} = \tilde{Z}_{j,k-1} - \tilde{Z}_{2j-1} \tag{14}$$

where the parameters a_2, a_1, b_0, and b_1 and the variance V are estimated in terms of the correlation coefficient ρ, which is independent of j and k, and of the HKP variance at level k (Koutsoyiannis 2002), as given by the following equations:

$$\begin{bmatrix} a_2 \\ a_1 \\ b_0 \\ b_1 \end{bmatrix} = \begin{bmatrix} 1 & \tilde{\rho}(1) & \tilde{\rho}(2)+\tilde{\rho}(3) & \tilde{\rho}(4)+\tilde{\rho}(5) \\ \tilde{\rho}(1) & 1 & \tilde{\rho}(1)+\tilde{\rho}(2) & \tilde{\rho}(3)+\tilde{\rho}(4) \\ \tilde{\rho}(2)+\tilde{\rho}(3) & \tilde{\rho}(1)+\tilde{\rho}(2) & 2[1+\tilde{\rho}(1)] & \tilde{\rho}(1)+2\tilde{\rho}(2)+\tilde{\rho}(3) \\ \tilde{\rho}(4)+\tilde{\rho}(5) & \tilde{\rho}(3)+\tilde{\rho}(4) & \tilde{\rho}(1)+2\tilde{\rho}(2)+\tilde{\rho}(3) & 2[1+\tilde{\rho}(1)] \end{bmatrix}^{-1} \begin{bmatrix} \tilde{\rho}(2) \\ \tilde{\rho}(1) \\ 1+\tilde{\rho}(1) \\ \tilde{\rho}(2)+\tilde{\rho}(3) \end{bmatrix} \tag{15}$$

and

$$VAR[V] = \tilde{\sigma}_k^2(1 - [\tilde{\rho}(2), \tilde{\rho}(1), \ 1+\tilde{\rho}(1), \tilde{\rho}(2)+\tilde{\rho}(3)][a_2, a_1, \quad b_0, b_1]^T \tag{16}$$

The mean and the variance in the HKP at the k-level of the cascade are

$$\tilde{\mu}_k = \langle \tilde{Z}_{j,k} \rangle = \frac{\Delta s_k}{f}\tilde{\mu}_0 = \frac{\tilde{\mu}_0}{2^k} \tag{17}$$

$$\tilde{\sigma}_k^2 = var[\tilde{Z}_{j,k}] = \left(\frac{\Delta S_k}{f}\right)^{2H} \tilde{\sigma}_0^2 = \frac{\tilde{\sigma}_k^2}{2^{2Hk}} \tag{18}$$

where $\Delta s_k = 2^{-k} f$ and H is HKP.

The above step-by-step disaggregation approach was introduced by Koutsoyiannis (2002), who established that it effectively generates fractional Gaussian noise. However, the precipitation process is not a Gaussian distribution. Indeed, specific exponentiation to the HKP is applied by the following equation to make a lognormal domain and preserve the scaling properties:

$$Z_{j,k} = \exp\left(\alpha(k)\tilde{Z}_{j,k} + \beta(k)\right) \tag{19}$$

HKP is assumed to be a unique process in the untransformed domain and the characteristics of the exponentiation transformation are changed for the transformed domain. Using different characteristics for different disaggregation steps while utilizing the scale-dependence of the daily step will help to transform the Gaussian domain to a lognormal domain by the following equations:

$$\alpha(k) = \frac{2^{Hk}}{\tilde{\sigma}_0}\sqrt{\ln(2^{2k(1-H)}(\exp\exp\left(\tilde{\sigma}_0^2 - 1\right) + 1)} \tag{20}$$

$$\beta(k) = -k\ln\ln 2 - \tilde{\mu}_0\left(\frac{\alpha(k)}{2^k} - 1\right) - \frac{\tilde{\sigma}_0^2}{2}\left(\frac{\alpha^2(k)}{2^{2Hk}} - 1\right) \tag{21}$$

The explained model is a disaggregation model only if the random variables are Gaussian processes. However, the hypothesis of lognormal rainfall, a conversion model of a coarser-scale into a small scale, is statistically consistent with the given process $\boldsymbol{Z}$ at the coarser-scale. The Hurst coefficient H is the only parameter of the HKP downscaling model. Therefore, the H value is estimated numerically.

H values have been estimated for each season from the historical time series because the disaggregated values are subject to the range of H values between 0 and 1. If the H value is closer to or beyond 1, the final values will be imagined, negative, or extreme. As a result, the simulated annual maximum precipitation (AMP) would be the effect. Therefore, the results are needed for the calibration procedure. The procedure is composed of thresholds and correction factors, which are estimated numerically using evolutionary optimization, such as a genetic algorithm, to estimate the optimal AMP values. The following equations illustrate the coefficients and thresholds, and these coefficients play the primary role in the results:

$$yy = pr_1 + pr_2 + pr_3 + pr_4 + x_4 \times R_{\text{sim}} \tag{22}$$

where

$$p_1 = 0.73 + \left(\frac{R_{\text{sim}}}{thr_1}\right) \tag{23}$$

$$p_2 = 0.12 + \left(\frac{R_{\text{sim}}}{thr_2}\right) \tag{24}$$

where

$$aa_1 = x_2 \times \left(\frac{R_{\text{sim}}^2}{thr_2}\right) \quad \text{and} \quad aa_2 = \frac{x_1 \times p_1 \times thr_1}{p_2} \tag{25}$$

$$pr_1 = x_{12} \times \sin\left(2\pi \times x_{11}\right) \tag{26}$$

$$pr_2 = x_1 \times thr_1 \times x_8^{1.99} \tag{27}$$

$$pr_4 = x_3 \times \frac{R_{\text{sim}}}{thr_2} \times R_{\text{sim}} \times x_{10}^{1.99} \tag{28}$$

$$pr_3 = aa_1 \times aa_2 \times x_9^{1.99} \tag{29}$$

Because the discrete data (precipitation to be simulated) are manipulated as samples of an analogue signal with its local maxima and minima of the AMP values, in some time intervals (some seasons), the coefficient performs as a periodic (distorted) signal with some periodicity.

The first poly (pr_1) contains a sinusoidal component, the factors play a role in the amplitude and phase (x_{12} manages the amplitude, and x_{11} controls the frequency of the sinusoidal component). The second poly (pr_2) has a *DC* value (direct current or constant value) where the simulated date is raised or lowered based on the factor value (x_1, x_8, and threshold [*thr1*]). The third poly (pr_3) is added to cover the linear component (x_4). The fourth poly (pr_4) is added to consider a square component where the observed data are squared and multiplied linearly by the factors (x_3 and x_{10}). In the last poly, a cubic component of the actual data is applied to cover more possibilities of correlation with the actual data (x_2, thr_2, x_1, and x_9).

2.4.4. The MRC model

The MRC model is a temporal scaling method that converts the time series from a coarse to a fine scale. Also, the conversion is based on branch splitting of each value at a daily or sub-daily scale. Therefore, the best branch splitting occurs when the original value is split into two cells, called a dyadic cascade. Then, the final format of the disaggregated hourly series comprises consecutive tree vertices of each rainy-day event.

In this section, *Pr* or *R* is the precipitation average over the timescale at the time origin ($j = 1$). *Pr* is assumed to be a random variable with a mean u_0 and variance $sigma_2$ of a stochastic process.

The branching number, which estimates the number of branches assigned to the next level with the smaller timescale steps for the distributed rainfall from the coarser-scale time step, is a structural component of the model. Using $b = 2$ means that the 24 h of the day could be split into day and night hours. Similarly, the day's hours could be split into morning and afternoon hours. The precipitation amount V is multiplied by multiplicative weights W_1 and W_2 to obtain V at each time step. The total summation of these weights must equal 1 at each level and they are not independent of one another; therefore, there is a probability of how the total amount of precipitation in each cascade level is converted. The following equation illustrates the three cases of each cascade level of branching ($b = 2$):

$$W_1, W_2 = \begin{cases} 0 \text{ and } 1 \text{ with } P(0/1) \\ 1 \text{ and } 0 \text{ with } P(1/0) \\ x \text{ and } 1-x \text{ with } P(x/(1-x));\ 0 < x < 1 \end{cases} \tag{30}$$

P denotes the probability for each time step in the level. The first case, which is P (1/0), means that the total precipitation is assigned in the first time step ($W_1 = 1$), and no precipitation will be allocated to the second time step when ($W_2 = 1 - W_1 = 0$). The probability of the P (0/1) disaggregation level is accomplished for the second case. The third case, which is the probability ($x/(1-x)$ splitting, is to redistribute the rainfall amount over the time step, where x is defined as $0 < x < 1$, and it represents the relative fraction of precipitation values that is attributed to the first step. The x value is a random variable in all disaggregation steps, and the PDF $f(x)$ can be estimated for each value of x. These cases in Equation (30) provide the following four different types of wet boxes with $Pi > 0$: the first box is the starting box, including a dry box in the past time step and a wet box in the later time step. Second, the ending box follows a wet box and is followed by the dry box; this can be called a chain box. Next, the isolated box is defined as side-by-side past boxes, and the next steps are dry. Finally, the enclosed box is an isolated box case, but it is for wet boxes.

A reverse scaling procedure achieved these probability cases for three different cases in Equation (29). Backward cascade level branching assumptions lead to highly resolved precipitation time series aggregation. Each cascade level of branches is summed to represent the total volume of precipitation at the preceding higher-level. The statistics (mean, maximum, minimum, and standard deviation) and probabilities are calculated for each branch in the level by dividing the counts of each case by the total number of elements of the higher cascading level time series. Additionally, statistical calculations are needed to evaluate the case $P(x/1-x)$, where x is the relative weight. Therefore, the relative weight (x) is a value between zero and the 90th percentile, influenced by the mean and standard deviation. This process aggregates the rainfall as follows: $1 \rightarrow 3$ h ($3{*}2^0$ h), $3 \rightarrow 6$ h ($3{*}2^1$ h), $6 \rightarrow 12$ h ($3{*}2^2$ h), and $12 \rightarrow 24$ h ($3{*}2^3$ h). In each aggregation step, a related weight is assigned to probabilities P (0/1), P (1/0), and P ($x/(1-x)$) before estimating the averages of all probabilities of all steps (Güntner *et al.* 2001). As a result, the probability and weight matrices are derived to represent the station's scaling. Notably, an empirical distribution is applied to estimate the parameters, which is done by a random number generator if there is no representation.

Sequentially, the weight matrices are applied to disaggregate the daily time series of precipitation. Tracing the random numbers for each cascade level, which incorporates the probabilities *(P* (0/1), *P* (1/0), and *P* $(x/(1-x))$) (they are cumulatively evaluated), defines the branching type in each time step.

When the disaggregation of the daily precipitation model begins, the drawing of the random numbers determines the type of branching that incorporates the probabilities (three cases in the above equations). If the random numbers are in the range $P(x/(1-x))$, a similar technique is applied to estimate the weight x value by using another random number.

A numerical simulation of the cascade is carried out if $\mu_o = 1$ and $a_o^2 = 0$. Thus, the summary statistics are

$$R_j^{(\Delta S_k)} = R_{j,k} = R_{1,0} \prod_{i=0}^{k} W_{g(i,j),i} \tag{31}$$

where $j = 1, 2, \ldots, b^k$ is the position index in the series at level k; i is the index of the cascade level; and $g(i, j)$ represents a function defining the position in the series at level i, i.e., $g(i,j) = \frac{j}{b^{k-i}}$, which is a ceiling function (Gaume *et al.* 2007). For $k = 0$, we have $W_{1,0} = 1$.

$$\frac{1}{b^k} \sum_{j=1}^{b^k} R_{j,k} = R_0 \tag{32}$$

where $< >$ denotes the expected value, which is an average over the independent realizations of the stochastic process. The expected value of $R_{j,k}$ is given by

$$R_{j,k} = R_k = R_{1,0} \prod_{i=0}^{k} W_{g(i,j),i} = R_0 \prod_{i=0}^{k} W_{g(i,j),i} = R_0 W^k = \mu_0 \mu_W^k \tag{33}$$

For a microcanonical cascade model, the k-level's mean process equals the process at the 0 level, which means that a further cascade level relationship will hold for every pair of successive aggregations.

$$\frac{1}{b} \sum_{i=b(j-1)+1}^{b-j} R_{j,k} = R_{j,k-1} \tag{34}$$

where $j = 1,\ldots\ bk - 1$ with $k > 0$. The following example explains how the microcascade model processes during each cascade level when $b = 2$:

$$\frac{1}{2} \sum_{i=2j-1}^{2j} R_{j,k} = R_{j,k-1},\ R_{2j-1,k} + R_{2j,k} = 2R_{j,k-1},\ W_{2j-1,k} = 2 - W_{2j,k} \tag{35}$$

Therefore, in the above equation, the weights $W_{j,k}$ fulfil $\mu_W = 1$ and $W < b$.

Let us assume that the branching value is $b = 2$, and the exponent $h_{j,k}(t)$ represents the top of the tree, excluding the cascading level start that belongs to both simple paths leading to $R_{j\ k}$ and $R_{j+t,k}$. The $h_{j,k}(t)$ *is* calculated as follows:

$$h_{j,k}(t) = \begin{cases} \sum_{r=1}^{k} \Theta[2^{r-1} - j - t], & j \le 2^k, t > 0 \\ h_{2^{k-j-t}+1,k}\ (t), & j > 2^k, t > 0 \\ h_{2^k-j+1,k}(|t|), & t < 0 \end{cases} \tag{36}$$

The following Equation (37) illustrates the computation of the model's exponent $h_{j,k}(t)$. In the computation, we use this equation: $\langle R_{j,k} R_{j+t,k} \rangle = \langle R_0^2 \rangle \langle W^2 \rangle^{h_{j,k}(t)}$. The arrows show the links to those variables considered, where $\Theta[n]$ is the discrete

form of the Heaviside step function, defined for a discrete variable (integer) n as

$$\Theta[n] = \begin{cases} 0, & n < 0 \\ 1, & n \geq 0 \end{cases} \quad < R_{j,k} R_{j+1,k} > = < R_{1,0}^2 >< W^2 > h_{j,k}(t) \tag{37}$$

$$< R_{4,3} R_{5,3} > = < W_{4,3} W_{2,2} W_{1,1} W_{5,3} W_{3,2} W_{2,1} R_{1,0}^2 > = < R_{1,0}^2 > \\ h_{4,3}(t = -1) = 2 \tag{38}$$

$$< R_{4,3} R_{5,3} > = < W_{4,3} W_{2,2}^2 W_{1,1}^2 W_{3,3} R_{1,0}^2 > = < R_{1,0}^2 >< W^2 2 > \\ R_{3,3} = W_{3,3} W_{2,2} W_{1,1} R_{1,0} \\ R_{4,3} = W_{4,3} W_{2,2} W_{1,1} R_{1,0} \\ R_{5,3} = W_{5,3} W_{3,2} W_{2,1} R_{1,0} \tag{39}$$

The mathematical part can be calculated numerically in the following section. The numerical experiment of the MRC model is explained by the following equation:

$$\rho_{j,k}(t) = \frac{(1 + \sigma_W^2)^{h_{j,k}(t)} - 1}{(1 + \sigma_W^2)^k - 1} \tag{40}$$

The weights W refer to the lognormal distribution defined as in the following equation:

$$W = b^{\sigma_N Y - \frac{\sigma_N^2 \ln b}{2}} \tag{41}$$

where Y is a normal random variable $N(1,0)$. Therefore, the variance in the weights is given by the following equation:

$$\sigma_W^2 = \exp(\sigma_N^2 (\ln b)^2) - 1 \tag{42}$$

where σ_N^2 is a parameter defining the standard random variable of normal distribution. To summarize, as the simulated sub-daily scale is essential for the storm control design system, this section elaborates on the mathematical scheme of the open-source software in which the MRC model was implemented. The model makes valuable contributions to water resource engineering.

2.5. Estimation of intensity-duration-frequency curves

The extreme theoretical value (EV) distribution approach estimates the frequency of extreme precipitation for different durations and return period events. The Gumbel type I distribution is

$$G(x; \mu, \beta) = \frac{1}{\beta} e^{\frac{x - \mu}{\beta}} e^{-e^{\frac{x - \mu}{\beta}}} \tag{43}$$

where μ is the location and β is the scale parameter. The random variable X_T associated with the return period can be estimated as in the following equation:

$$X_T = \bar{X} + K_T S \tag{44}$$

where $\bar{X}$ is the mean of the observed or simulated AMP values and S is the standard deviation. K_T is the frequency factor calculated with a given return period (T):

$$K_T = -\frac{\sqrt{6}}{\pi} \left[0.5772 + \ln\left(\ln\left(\frac{T}{T - 1} \right) \right) \right] \tag{45}$$

The duration events of 1–24 h are used and the return periods of 2-, 5-, 10-, 50-, and 100-year are chosen to construct the curves.

3. RESULTS

The uncorrected outputs of the four RCMs were downscaled using QM at the four climate stations on four arbitrarily chosen periods: a historical period (1979–2005), a short-term period (2011–2040), a medium-term period (2041–2070), and a long-term period (2071–2100). Each of the 64 daily time series was temporally disaggregated using five techniques (HKP, MRC, FO, and KNN using 5, 15, and 30 neighbours). When using HKP and MRC, the daily time series were temporally disaggregated on five levels to obtain a time step of 1/36 h. These time series were linearly interpolated to produce hourly time series. Each hourly time series was afterwards aggregated to obtain precipitation intensity time series at a 2, 3, …., and 24 h time step, which in turn were converted into 24 h time series of annual maximums and an IDF curve. The performance of each disaggregation time series was assessed by (a) comparing the time series of annual maxima to corresponding observations using box plots and the KS test and (b) comparing the IDF curves derived from temporally disaggregated data with the IDF curves generated by observations on the historical period. The results of these comparisons are presented in the following sections:

3.1. Comparison of the simulated and observed time series of each temporal downscaling method

Figure 4 compares the observed and the disaggregated annual maxima resulting from the FO, KNN (5), KNN (15), KNN (30), HKP, and MRC models in the historical period for the 1 and 24 h time series. None of the models perfectly captures the interquartile range of the observed data, as it was generally underestimated by MRC but overestimated by the KNN models, HKP and FO at the 1 h time step. Almost all models overestimated the interquartile range for 24 h time series, while HKP did not

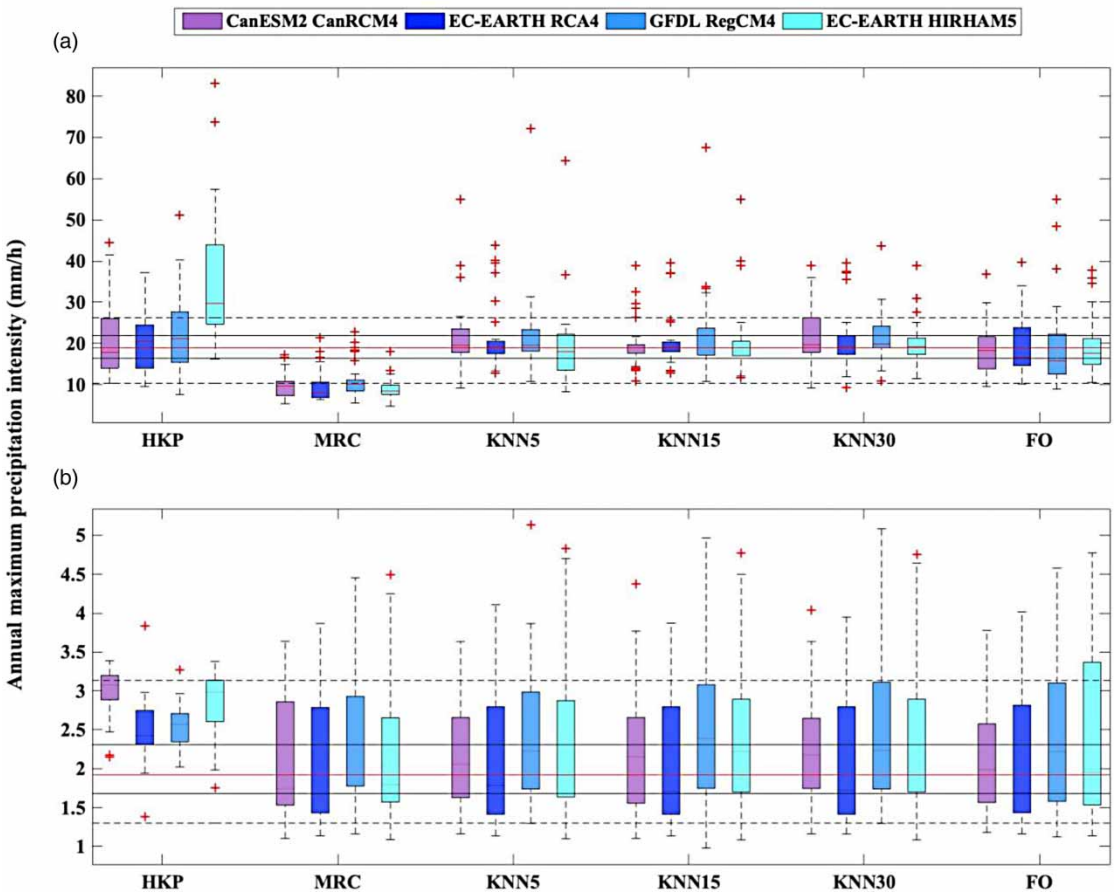

Figure 4 | Grouped boxplot for all disaggregation methods and different RCMs in the historical period using (a) 1 h precipitation data, and (b) 24 h precipitation data. The horizontal solid black lines represent the 25th and 75th percentiles while the horizontal solid red line represents the 50th percentile of the observed data. The dashed lines represent the whiskers (extended to the most extreme data points not considered outliers) of the observed data. The outliers are shown as '+' marker symbol.

mimic the observed values regardless of the RCM used. Results also show that HKP and MRC lead to more severe biases: HKP overestimates precipitation intensity at the 1 h time step, while MRC underestimates it at the 24 h time step. FO performed well compared to other models in terms of bias and interquartile range. The main descriptive statistics for each model, namely the mean, standard deviation, kurtosis, and skewness, are presented in Table 2. All methods have mean and standard deviation values of the historical period close to the observations, while there are deviations in the kurtosis and skewness coefficients. The skewness of the observation and the FO and KNN models (all neighbour sizes) were found to be relatively similar to those of the observed values. MRC and HKP, in contrast, underestimated the skewness and the kurtosis values.

Table 3 provides the results of the similarity percentage between observed and downscaled AMP in the calibration and validation periods. The similarity percentage is estimated based on each climate station's KS test results of each temporal

Table 2 | Descriptive statistics of observed and disaggregated hourly time series of Russell Station

Disaggregation method	GCM, RCM	Mean	Standard deviation	Skewness	Kurtosis
Observed	–	**0.1**	**0.6**	**20.7**	**760**
HKP	CanESM2, CanRCM4	0.1	0.5	7.1	82.4
	EC-EARTH, HIRHAM5	0.1	0.4	8.6	139.8
	EC-EARTH, RCA4	0.1	0.4	7.8	108.1
	GFDL, RegCM4	0.1	0.6	21.9	679.5
MRC	CanESM2, CanRCM4	0.1	0.4	9.9	150.4
	EC-EARTH, HIRHAM5	0.1	0.5	11.9	283.7
	EC-EARTH, RCA4	0.1	0.5	9.9	152.5
	GFDL, RegCM4	0.1	0.5	11.8	244.5
KNN(5)	CanESM2, CanRCM4	0.1	0.6	18.4	5,613
	EC-EARTH, HIRHAM5	0.1	0.4	18.2	526.4
	EC-EARTH, RCA4	0.1	0.6	18.9	516.7
	GFDL, RegCM4	0.1	0.6	22.8	782.5
KNN(15)	CanESM2, CanRCM4	0.1	0.6	21.7	885.2
	EC-EARTH, HIRHAM5	0.1	0.4	18.4	539.7
	EC-EARTH, RCA4	0.1	0.6	18.2	475.6
	GFDL, RegCM4	0.1	0.7	24.8	910.4
KNN(30)	CanESM2, CanRCM4	0.1	0.6	19.5	636.5
	EC-EARTH, HIRHAM5	0.1	0.4	18.3	535.2
	EC-EARTH, RCA4	0.1	0.6	18.8	507.3
	GFDL, RegCM4	0.1	0.8	24.9	756.5
FO	CanESM2, CanRCM4	0.1	0.6	15.6	394
	EC-EARTH, HIRHAM5	0.1	0.4	11.9	196.1
	EC-EARTH, RCA4	0.1	0.6	14.3	264.9
	GFDL, RegCM4	0.1	0.7	27.6	1,112.5

Bold indicating the reference point for comparison (Observed Data).

Table 3 | Percentage of similarity between observed and downscaled AMP in the calibration (*Cal.*) and validation (*Val.*) periods across all climate change models

Station	Russell		Morrisburg		St. Albert		South Mountain	
Model	*Cal.* (%)	*Val.* (%)	*Cal.* (%)	*Val.* (%)	*Cal.* (%)	*Val.* (%)	*Cal.* (%)	*Val.* (%)
HKP	63	50	65	70	63	60	20	60
MRC	0	0	0	60	0	10	10	60
KNN 5	63	88	94	100	60	55	80	100
KNN 15	65	100	100	100	65	100	100	100
KNN 30	75	100	100	100	75	100	100	100
FO	100	100	94	100	100	100	100	100

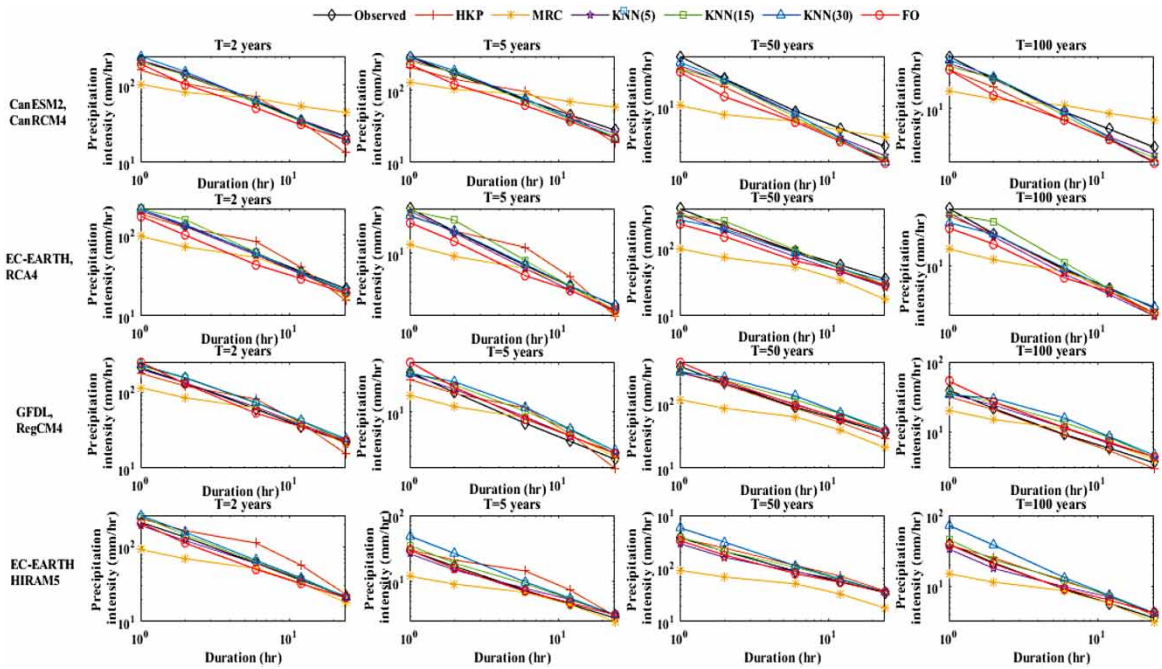

Figure 5 | IDF curves at the Russell Station for all disaggregation methods using different RCMs in the historical period for the return period of 2, 5, 50, and 100 years.

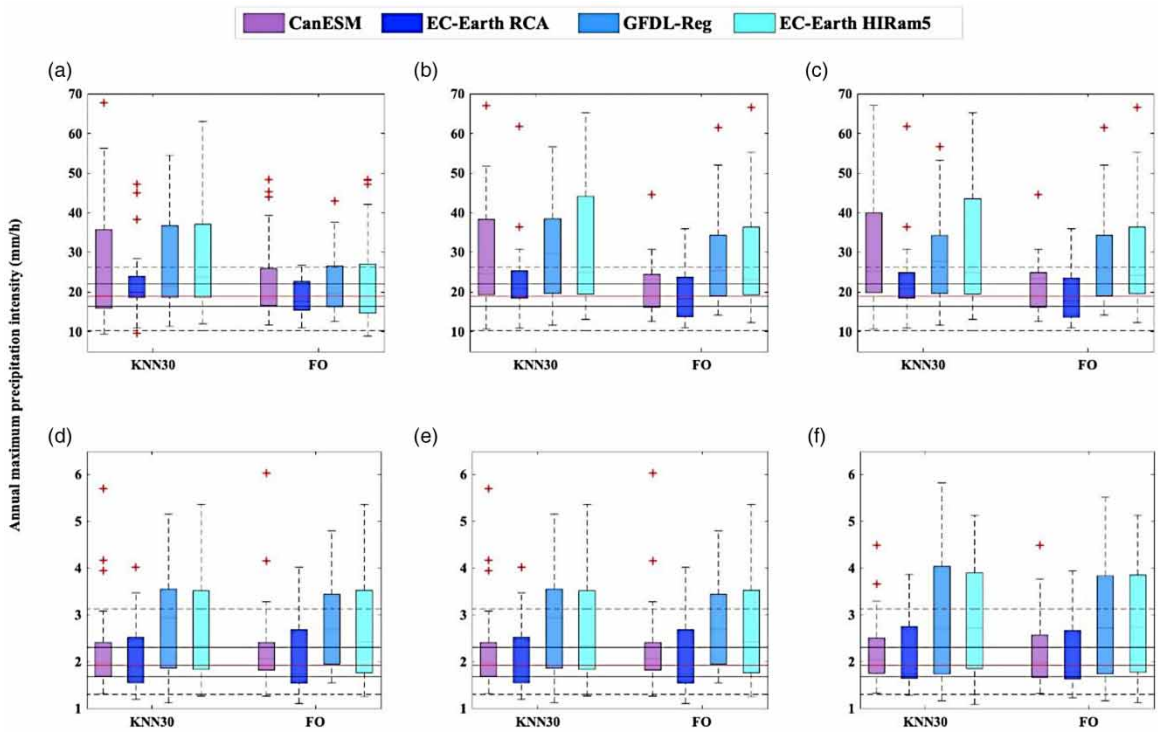

Figure 6 | Grouped boxplot for KNN(30) and FO disaggregation methods and different RCMs in the future periods using (a) 1 h precipitation data in the short-term period; and (b) 1 h precipitation data in the medium-term period; and (c) 1 h precipitation data in the long-term period. (f) 24 h precipitation data in the short-term period, and (e) 24 h precipitation data in the medium-term period, and (d) 24 h precipitation data in the long-term period. The horizontal solid black lines represent the 25th and 75th percentiles while the horizontal solid red line represents the 50th percentile of the observed data. The dashed lines represent the whiskers (extended to the most extreme data points not considered outliers) of the observed data. The outliers are shown as '+' marker symbol.

downscaling. The null hypothesis was systematically rejected for the MRC, except for the 1 h duration event accepted by the test (the Russell Station, duration = 1 h) with a very small *p*-value, i.e., close to rejection. HKP had 20 and 70% acceptance rates, while KNN and FO had better acceptance rates. KNN (30) and FO had acceptance rates of 100% except for one station, making them the best disaggregation techniques in this study.

3.2. Comparison of the generated IDF curves of each temporal stochastic downscaling method

The IDF curves generated using observations and disaggregated time series on the historical period are shown in Figure 5, representing one sample station, namely Russell Station. IDF curves for the same station on the long-term period are shown in Figure 6 (next section). The IDF curves have been generated using AMP generated using all temporal stochastic disaggregation models for each return period of 2-, 5-, 10-, 50-, and 100-year events in the historical period and three future climate periods (short-term: 2011–2040, medium-term: 2041–2070 and long-term: 2071–2100). Figure 5 shows that the IDF curves generated by KNN models and FO are generally closer to the IDF curves of observations than those generated using HKP and MRC. KNN (30) and FO are competing for first place. For two RCMs (CanESM2, CanRCM4, and EC-EARTH HIRHAM5), disaggregation using KNN (30) leads to the most realistic IDF curves. For the two others (EC-EARTH RCA4, GFDL RegCM4), FO seems to be the best.

4. DISCUSSION

The increasing intensity and frequency of extreme urban precipitation have been reported in the literature due to a changing environment. Short-duration extreme precipitation, in particular, is expected to become increasingly severe in many areas. As a result, the traditional frequency analysis method's underlying assumption for generating IDF curves has been called into question (Qu *et al.* 2020; Yan *et al.* 2020; Cook *et al.* 2020). Furthermore, the covariate-based nonstationary model can be used to generate future IDF (Yan *et al.* 2021).

Given that sub-daily, finer-scale precipitation time series are essential for stormwater control and management in urban water systems, an efficient temporal disaggregation method is crucial due to the lack of such data in some locations. The input of disaggregated or projected IDF to the urban water management model is one of the most crucial applications to

Table 4 | Summary of results

Temporal disaggregation method	Preservation of descriptive statistics in the generated hourly time series	Comparison of the generated annual maximums to observations using boxplots	Percentage of similarity of annual maximum time series using KS test	Comparison of IDF curves generated with disaggregated time series to IDF curves of observations
MRC	Mean and standard deviation preserved, underestimate skewness and kurtosis	Underestimates interquartile range and mean intensity at the 1 h time step	Systematic rejection	Significantly deviates from the IDF of observations
HKP	Mean and standard deviation preserved, underestimate skewness and kurtosis	Underestimates interquartile range and overestimates mean intensity at the 24 h time step	Acceptance rate ranging from 20 to 70%	Significantly deviates from the IDF of observations
FO	Mean and standard deviation preserved, moderate underestimation of skewness. Kurtosis is generally underestimated (three out of four RCMs)	Interquartile range overestimated; reasonable estimation of mean intensity compared to MRC and HKP. Similar to KNN	The acceptance rate is generally 100%, except for one station where it is 94%	Generally close to the IDF of observations
KNN	Mean and standard deviation preserved, reasonable estimation of skewness and kurtosis	Interquartile range overestimated; reasonable estimation of mean intensity compared to MRC and HKP. Similar to FO	Acceptance rate increase with neighbourhood. Generally, 100% for a neighbourhood of 30, except for two stations where it is 75%	Generally close to the IDF of observations. Agreement increases with the size of the neighbourhood.

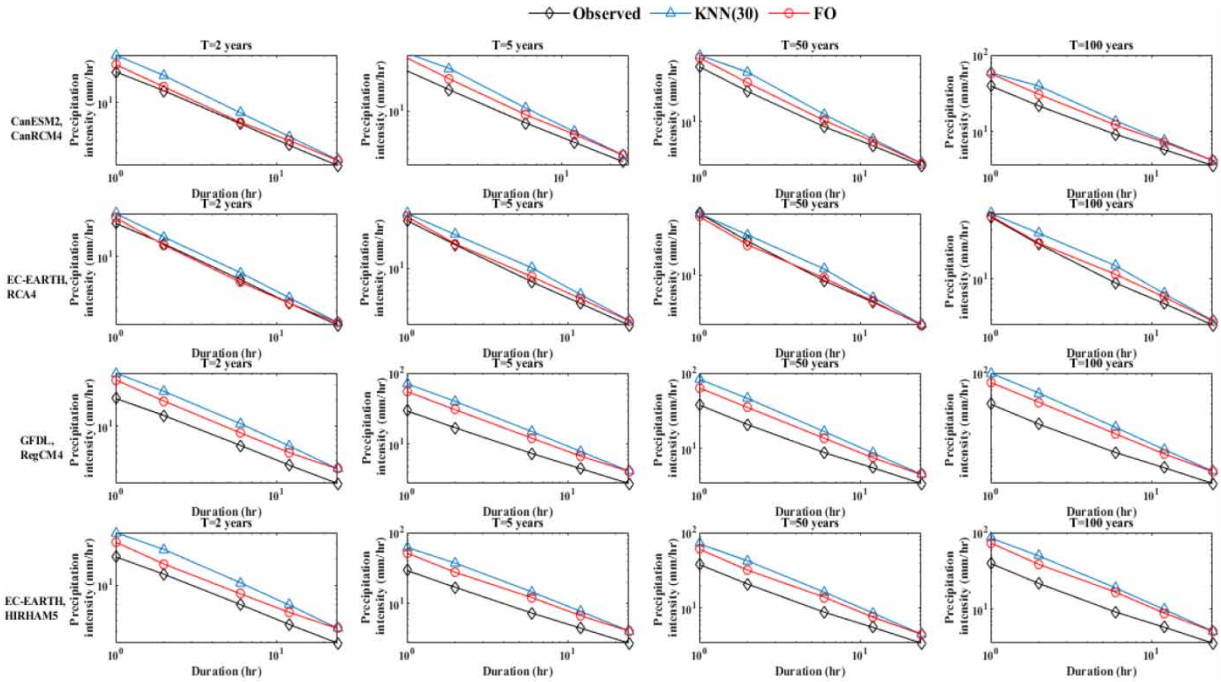

Figure 7 | IDF curves of Russell Station curves resulting from KNN 30 and FO disaggregation methods, long period (all climate models); for return periods $T = 2$, 5, 50, and 100 years.

analyse further the effects of climate change on local urban floods (Xiong *et al.* 2019). The sub-daily time series can be directly used in rainfall–runoff models or transformed into IDF curves using the rational method. Six different temporal disaggregation models (the KNN disaggregation with neighbour sizes of 5, 15, and 30, the HKP, the MRC, and the proposed FO model) were applied to the downscaled precipitation time series of four climate stations in the South Nation watershed. Various tests were used to assess the performance of the temporal disaggregation techniques. The main findings are recapitulated in Table 4.

All methods preserved the main descriptive statistics, such as the mean and standard deviation of the precipitation intensity. The three last comparison methods all seem to suggest that FO and KNN (30) are the most appropriate temporal disaggregation methods for the study area. Note that these results cannot be generalized and that different results could have been obtained if other climate stations or RCMs were used. It is also worth noting that the parameters of MRC and HKP were obtained by optimization, and its algorithm could have affected the final performance of the methods. The box plots of the projected precipitation intensities using the two best methods (FO and KNN (30)) are shown on Figure 6. Figure 7 shows the corresponding IDF curves. All figures suggest precipitation intensities will increase in the future in the study area, potentially making urban water infrastructure less safe as the impacts of global warming kick in.

This study highlights the importance of carefully selecting the method used to generate future IDF curves, as two different methods can yield wildly different results. The resilience of urban infrastructure, public safety, and global economic prosperity in the future are at stake and the blind use of a particular method can lead to maladaptation and costly infrastructure failure.

5. CONCLUSIONS

Given that precipitation projections are typically at a daily time scale, temporal disaggregation using techniques of variable complexity is often needed to evaluate the risk/performance of urban infrastructure in the future. Temporal disaggregation techniques have different levels of complexity and unequal performances, and the generated time series may not have the same statistical characteristics. In this paper, a simple steady-state stochastic disaggregation model that generates wet/dry day occurrence using a binomial distribution and precipitation intensity using an exponential distribution is proposed and compared to widely used temporal disaggregation methods: the MRC model, the HKP, and three versions of the KNN

model using the nonparametric KS test. Daily time series of future precipitation are generated by temporally downscaling the outputs of four RCMs using the QM method. Results show that for the selected RCMs and climate stations, while all methods can preserve descriptive statistics in the hourly time series, they perform very differently when it comes to the annual maximum time series. The annual maximum time series generated using MRC systematically failed the KS test comparing them to observations, while HKP had low (20–70%) acceptance rates. FO and KNN (30) had acceptance rates close to 100% and led to the most realistic annual maximum time series at sub-daily and IDF curves, suggesting that complexity does not necessarily yield the best results. This research emphasizes the necessity of choosing the appropriate approach for creating future IDF curves with caution, as the outcomes can differ significantly depending on the method employed. Furthermore, it should be noted that the findings of this study cannot be extrapolated to other locations and those alternate outcomes would have likely occurred had different climate regimes or RCMs been utilized.

DATA AVAILABILITY STATEMENT

Data cannot be made publicly available; readers should contact the corresponding author for details.

CONFLICT OF INTEREST

The authors declare there is no conflict.

REFERENCES

Alodah, A. 2015 *Development of Climate Change Scenarios for the South Nation Watershed*. Masters dissertation, University of Ottawa, Ottawa.

Alodah, A. & Seidou, O. 2019 Assessment of climate change impacts on extreme high and low flows: an improved bottom-up approach. *Water* **11** (6), 1236.

Alzahrani, F., Seidou, O. & Alodah, A. 2022 Assessment and improvement of IDF generation algorithms used in the IDF_CC tool. *Water Resources Management* **36**, 4591–4606.

Cook, L. M., McGinnis, S. & Samaras, C. 2020 The effect of modelling choices on updating intensity-duration-frequency curves and stormwater infrastructure designs for climate change. *Climatic Change* **159** (2), 289–308.

Garbrecht, J. D., Gyawali, R., Malone, R. W. & Zhang, J. C. 2017 Cascade rainfall disaggregation application in US Central Plains. *Environment and Natural Resources Research* **7** (4), 30–43.

Gaur, A. & Lacasse, M. 2018 Multisite multivariate disaggregation of climate parameters using multiplicative random cascades. *Urban Climate* **26**, 121–132.

Gaume, E., Mouhous, N. & Andrieu, H. 2007 Rainfall stochastic disaggregation models: Calibration and validation of a multiplicative cascade model. *Advances in Water Resources* **30**, 1301–1319.

Güntner, A., Olsson, J., Calver, A. & Gannon, B. 2001 Cascade-based disaggregation of continuous rainfall time series: the influence of climate. *Hydrology and Earth System Sciences* **5** (2), 145–164.

Hurst, H. E. 1951 Long-term storage capacity of reservoirs. *Transactions of the American Society of Civil Engineers* **116** (1), 770–799.

Jakob, D., Karoly, D. J. & Seed, A. 2011 Non-stationarity in daily and sub-daily intense rainfall – part 1: Sydney. *Australia. Natural Hazards and Earth System Sciences* **11** (8), 2263–2271.

Jebari, S., Berndtsson, R., Olsson, J. & Bahri, A. 2012 Soil erosion estimation based on rainfall disaggregation. *Journal of Hydrology* **436–437**, 102–110.

Koutsoyiannis, D. & Cohn, T. A. 2008 The Hurst phenomenon and climate (solicited). In: *European Geosciences Union General Assembly 2008, Geophysical Research Abstracts*. European Geosciences Union, Vienna, Austria, p. 11804.

Koutsoyiannis, D. & Onof, C. 2001 Rainfall disaggregation using adjusting procedures on a Poisson cluster model. *Journal of Hydrology* **246** (1), 109–122.

Koutsoyiannis, D. 2002 The Hurst phenomenon and fractional Gaussian noise made easy. *Hydrological Sciences Journal* **47** (4), 573–595.

Koutsoyiannis, D., Paschalis, A. & Theodoratos, N. 2011 Two-dimensional Hurst–Kolmogorov process and its application to rainfall fields. *Journal of Hydrology* **398** (1–2), 91–100.

Licznar, P., Łomotowski, J. & Rupp, D. E. 2011 Random cascade driven rainfall disaggregation for urban hydrology: an evaluation of six models and a new generator. *Atmospheric Research* **99** (3), 563–578.

Lombardo, F., Volpi, E. & Koutsoyiannis, D. 2012 Rainfall downscaling in time: theoretical and empirical comparison between multifractal and Hurst-Kolmogorov discrete random cascades. *Hydrological Sciences Journal* **57** (6), 1052–1066.

Lombardo, F., Volpi, E., Koutsoyiannis, D. & Serinaldi, F. 2017 A theoretically consistent stochastic cascade for temporal disaggregation of intermittent rainfall. *Water Resources Research* **53** (6), 4586–4605.

Lu, Y., Qin, X. S. & Mandapaka, P. V. 2015 A combined weather generator and K-nearest-neighbour approach for assessing climate change impact on regional rainfall extremes. *International Journal of Climatology* **35** (15), 4493–4508.

Molnar, P. & Burlando, P. 2005 Preservation of rainfall properties in stochastic disaggregation by a simple random cascade model. *Atmospheric Research* **77** (1), 137–151.

Müller, H. & Haberlandt, U. 2015 Temporal rainfall disaggregation with a cascade model: from single-station disaggregation to spatial rainfall. *Journal of Hydrologic Engineering* **20** (11), 04015026.

Olsson, J. 1998 Evaluation of a scaling cascade model for temporal rainfall disaggregation. *Hydrological Earth Systems Science* **2** (1), 19–30.

Olsson, J. & Berndtsson, R. 1998 Temporal rainfall disaggregation based on scaling properties. *Water Science and Technology* **37** (11), 73–79.

Park, H. & Chung, G. 2020 A nonparametric stochastic approach for disaggregation of daily to hourly rainfall using 3-day rainfall patterns. *Water* **12** (8), 2306.

Qu, C., Li, J., Yan, L., Yan, P. & Lu, D. 2020 Non-stationary flood frequency analysis using cubic B-spline-based gamlss model. *Water* **12** (7), 1867.

Sharif, M. & Burn, D. H. 2007 Improved K -nearest neighbor weather generating model. *Journal of Hydrologic Engineering* **12** (1), 42–51.

Sharif, M., Burn, D. H. & Hofbauer, K. M. 2013 Generation of daily and hourly weather variables for use in climate change vulnerability assessment. *Water Resources Management* **27** (5), 1533–1550.

Sharma, A. & Srikanthan, S. 2006 Continuous rainfall simulation: a nonparametric alternative. In: *30th Hydrology & Water Resources Symposium: Past, Present & Future: Past, Present & Future*. Conference Design, Sandy Bay, Tasmania, pp. 86–91.

Srikanthan, R., Sharma, A. & McMahon, T. 2006 Comparison of two nonparametric alternatives for stochastic generation of monthly rainfall. *Journal of Hydrologic Engineering* **11** (3), 222–229.

Tayşi, H. & Özger, M. 2022 Disaggregation of future GCMs to generate IDF curves for the assessment of urban floods. *Journal of Water and Climate Change* **13** (2), 684–706.

Uraba, M. B., Gunawardhana, L. N., Al-Rawas, G. A. & Baawain, M. S. 2019 A downscaling-disaggregation approach for developing IDF curves in arid regions. *Environmental Monitoring and Assessment* **191** (4), 245.

Wey, K. 2006 *Temporal disaggregation of daily precipitation data in a changing climate*. Master's thesis, University of Waterloo, Waterloo.

Xiong, L., Yan, L., Du, T., Yan, P., Li, L. & Xu, W. 2019 Impacts of climate change on urban extreme rainfall and drainage infrastructure performance: a case study in Wuhan City, China. *Irrigation and Drainage* **68** (2), 152–164.

Yan, L., Xiong, L., Luan, Q., Jiang, C., Yu, K. & Xu, C. Y. 2020 On the applicability of the expected waiting time method in nonstationary flood design. *Water Resources Management* **34** (8), 2585–2601.

Yan, L., Xiong, L., Jiang, C., Zhang, M., Wang, D. & Xu, C. Y. 2021 Updating intensity-duration-frequency curves for urban infrastructure design under a changing environment. *Wiley Interdisciplinary Reviews: Water* **8** (3), e1519.

Zhao, W., Kinouchi, T. & Nguyen, H. Q. 2021 A framework for projecting future intensity-duration-frequency (IDF) curves based on CORDEX Southeast Asia multi-model simulations: an application for two cities in Southern Vietnam. *Journal of Hydrology* **598**, 126461.

Zhu, J., Stone, M. C. & Forsee, W. 2012 Analysis of potential impacts of climate change on intensity–duration–frequency (IDF) relationships for six regions in the United States. *Journal of Water and Climate Change* **3** (3), 185–196.

First received 22 December 2022; accepted in revised form 14 March 2023. Available online 27 March 2023